Porous hollow cobalt-based oxides encapsulated with bimetallic PdAu Nanoparticles of electrochemical biosensor for highly sensitive pesticides detection

Yaxu Zhao
Tianjin University of Science and Technology
Lijun Liang
Tianjin University of Science and Technology
Wei Guo
Tianjin University of Science and Technology
Xiong Lu
Tianjin University of Science and Technology
Congyi Zhao
Tianjin University of Science and Technology
Faming Gao (fmgao@tust.edu.cn)
Tianjin University of Science and Technology

Research Article

Keywords: cobalt-based oxides, PdAu Nanoparticle, Organophosphorus pesticides

Posted Date: December 19th, 2022

DOI: https://doi.org/10.21203/rs.3.rs-2375797/v1

Abstract

Efficient and portable electrochemical biosensors are received to evaluation of pesticides in the environment, which can make great significance for food safety. In this study, the Co-based oxides with a kind of hierarchical porous hollow and nanocages were constructed, in which the materials (Co_3O_4-NC) were encapsulated with PdAu Nanoparticles (NPs). Due to the unique porous structure, the changeable valence state of cobalt and the synergistic effect of bimetallic PdAu NPs, PdAu@Co_3O_4-NC possessed excellent electron pathways, and showed more exposed active sites. Accordingly, the porous Co-based oxides have been applied to construct an activeacetylcholinesterase (AChE) electrochemical biosensor, which showed good performance for organophosphorus pesticides (OPs) detection. The optimum AChE-CS/PdAu@Co_3O_4-NC/GCE platform allows to exhibit highly sensitive determination of omethoate and chlorpyrifos, with the relative low detection limit of 6.125×10^{-15} M and 5.10×10^{-13} M, respectively. And a wide linear range of $6.125 \times 10^{-15} \sim 6.125 \times 10^{-6}$ M and $5.10 \times 10^{-13} \sim 5.10 \times 10^{-6}$ M for these two pesticides were also achieved. Therefore, the PdAu@Co_3O_4-NC may represent a powerful tool for ultrasensitive sensing of (OPs), and have great potential application.

Introduction

OPs were a common chemical agent used in agriculture to protect crops from worms and insects[1]. Over the last few decades, since the growing population and rapid urbanization, the use of OPs has increased globally, which may affect ecosystems, agricultural product safety and human health[2]. These OPs can destroy the biological function of AChE in nervous system that regulates the acetylcholine neurotransmitter in the cholinergic system[3, 4]. The AChE was inhibited that it lead to the acetylcholine accumulation in the neuro-synapse resulting in prolonged neuro-excitation, which may cause muscular dystrophy, neurological disorders, reproductive disorders, even lead to death[5, 6]. As a result, it is crucial to develop effective and sensitive pesticide detection methods. Currently, traditional pesticide detection methods included mass spectrometry (MS)[7], high performance liquid chromatography (HPLC)[8] and gas chromatography-mass spectrometry[9]. These methods can achieve qualitative and quantitative analysis, but cannot meet the on-site detection requirement[10]. Notably, AChE inhibition-based biosensors have gotten attractive attention due to their simplicity, high sensitivity, and relatively low cost [11]. Enzyme inhibition-based method is depended on that OPs can inactivate the AChE by phosphorylation of the serine residue from the catalytic triad in the AChE active center. And this would result in a decrease in the production of thiocholine (TCl), which was generated from the hydrolysis of acetylthiocholine chloride (ATCl) by AChE. TCl was an electroactive substance and can be oxidized to produce an oxidation current at a certain voltage, which can be used as a label for the detection of OPs[12].

New nanomaterials have been used in electrochemical sensors for more than a decade. Many of the research efforts have been directed toward applying the adjustable materials including Metal-organic frameworks (MOFs), graphene, or MXene[13–15]. The MOFs with unique properties have been used as

precursors with possibility of post synthetic modifications and stability. Liu et al.[16] prepared a robust ratiometric fluorescent nanosensor base on NH_2-MIL-101(Fe), exhibiting unusually high performance to assay carbaryl. Notably, MOF-derived transition metal oxides may create better catalytic performance due to valence changes. Variable metal between two valence states had suitable redox properties and could speed up electron transfer. For instance, Ce^{4+}/Ce^{3+} redox pairs can be used as charge transfer media to promote electron transfer and demonstrate a sensitive detection of paraoxon.[17, 18]. Moreover, certain Co-MOF derivatives (e.g., Co_3O_4), have gained prominence for better electrochemical performance, owing to a redox reaction could occur from Co^{3+} to Co^{2+} and/or accelerated catalysis versus Co-MOF[19, 20]. Surprisingly, in these systems, the attractive features of Co_3O_4 suggested tremendous promise for the higher oxygenophilic increased the affinity and adsorption of ATCl [21]. Meanwhile, MOFs had a good prospect in stabilizing nanoparticles, and the inner and outer layer structures of the materials exhibit synergistic effected for better electrochemical performance[22]. Wang et al.[23] made gold nanoparticles decorated zeolitic imidazolate frameworks (Au-ZIF-8) that was employed to fabricate biosensor for protein kinase A activity assay. Notably, noble metal particles were suitable as modified electrode materials, because of their high conductivity and catalytic activity. Additionally, bimetallic nanomaterials have higher specific surface area and synergy, better catalysis, conductivity and luminescence than single metal nanoparticles, and are widely used in the field of sensors[24]. Lu et al. [25] synthesized one-dimensional bimetallic Pd@Au core-shell nanorods and constructed a highly sensitive AChE biosensor for the detection of OPs.

Herein, PdAu@CoMOF-NH_2 nanocomposites were synthesized and treated at annealing to form a Co-based oxide with a hollow structure for the detection of OPs. The PdAu@Co_3O_4-NC have preferable biocompatibility, excellent catalytic activity. The conversion of ATCl to TCl was promoted by using the synergistic effect of AChE immobilized on the electrode with the double-shell amorphous Co_3O_4. Meanwhile, the Co_3O_4-NC were modified by PdNPs and AuNPs, which promoted the catalysis of TCl (with functional group of -S-H-) to generate dithio-bis-choline (-S-S-), thereby generating an oxidation current[26, 27]. At the same time, PdAu@Co_3O_4-NC shortened the electron transfer route, which further effectively improved the amplification of the electrocatalytic signal. Overall, this work not only provided a new and innovative method to design double-shelled and porous Co_3O_4-NC loaded bimetallic PdAuNPs to constructe AChE biosensor, but also showed a sensitive and efficient electrochemical strategy for OPs detection.

2. Experimental

2.1. Material And Apparatus

Gold chloride ($HAuCl_4$), potassium chloropalladate(II) (K_2PdCl_4), 2-aminoterephthalic acid (NH_2-BDC), cobaltous. nitrate hexahydrate ($Co(NO_3)_2{\cdot}6H_2O$), N,N-dimethylformamide (DMF), sodium borohydride ($NaBH_4$), AChE (from electric eel), acetylcholine chloride (ATCl), chitosan (CS), naphthol, 2-methylimidazole (H-MeIM), omethoate, chlorpyrifos Standard, Methanol (AR) and ethanol (AR) are

purchased from Shanghai Aladdin Co., Ltd. Phosphate buffffered saline (PBS) is prepared by using Na_2HPO_4 and NaH_2PO_4 solution. $K_3Fe(CN)_6/K_4Fe\ (CN)_6$ and KCl solution are used as electrolyte for electrochemical impedance spectroscopy (CV and EIS).

Transmission electron microscope (TEM, FEI Telos F200X, USA), high-resolution TEM (HRTEM, FEI Tecnai F30). The morphologies and composition of nanomaterials (SEM, FEI Apreo, USA), X-ray diffraction (XRD, Rigaku D/MAX-2500). CHI660E electrochemical workstation (Shanghai Chen Hua Instrument, China) for electrochemical testing. Adopting three-electrode system by using a platinum wire as counter electrode, the glassy carbon electrode as work electrode (GCE) and a saturated calomel electrode as reference electrode (SCE).

2.2. Synthesis Of Comof-nh

The synthesized method of ZIF-67 crystal was reported by Sara Rafiei et al.[28], and the synthesis step has been slightly improved. In details, 2 mmol $Co(NO_3)_2{\cdot}6H_2O$ and 6 mmol H-MeIM were dissolved into methanol (30 mL) solution respectively. And then the $Co(NO_3)_2{\cdot}6H_2O$ mixing of solutions was slowly added to the H-MeIM solution with continuously stirring to evenly mix the solution with the condition of room temperature for 8 hours. After centrifugation, it was washed with methanol and water five times. The collected centrifuged material was dried in the vacuum drying oven at 60℃/10 h, and the product of ZIF-67 was obtained.

To prepare the CoMOF-NH_2, 18.8mg ZIF-67 and 0.03024g NH_2-BDC with a solvothermal method in DMF. NH_2-BDC was dissolved in methanol, and then 20 ml of ZIF-67 was added dropwise to the NH_2-BDC mixture every five minutes and left to stir at room temperature for 3 hours. The stirred mixed solution is transferred to the autoclave and the solvent heat reaction is carried out at 100℃/10 h. When the reaction was finished, the precipitate was repeatedly washed with distilled water, collected by centrifugation and dried at 60℃/10 h.

2.3. Synthesis Of Pdau@comof-nh And Pdau@coo-nc

PdAu@CoMOF-NH_2 was synthesized as the follows. First of all, 50 mg CoMOF-NH_2 and a certain amount of K_2PdCl_4 (500µl, 2.5mM) aqueous solution were put in a small beaker. Subsequently, added 2ml of methanol to the above mixture, and stirred to make it evenly mixed. It was then transferred to a porcelain crucible and heated at a temperature of 70℃ to evaporate the solution. To give Pd^{2+}/CoMOF-NH_2, this experimental procedure was repeated several times. The Pd^{2+}/CoMOF-NH_2 sample was then dispersed into 5 mL of MeOH by sonication, and $NaBH_4$ (500µL, 5mM)was added while stirring. The $NaBH_4$ solution was then slowly added dropwise to the above mixture, allowing it to react completely. The obtained product was washed with methanol, heated to 60°in a water bath, and $HAuCl_4$ aqueous solution(500µL, 5mM) was slowly added to it. The prepared product was washed several times with MeOH, and then

centrifugalized until the supernatant liquid became colorless. The product was dried in a vacuum oven at 60℃ for 12 h. Finally, the sample (PdAu@Co_3O_4-NC) of 100 mg was placed in a muffle furnace and treated at 300℃ for 2 h in the air to obtain.

2.4. Preparation Of Ache-cs/pdau@coo-nc/gce

In brief, 5 μL of PdAu@Co_3O_4-NC suspension (diluted to 0.25 mg·mL^{-1} with deionized water) was mixed with naphthol and dropped onto the electrode surface prepared in advance. The treated electrodes are left to dry in natural conditions. Then, 1 μL of AChE (0.2 U· μL^{-1}) and 4 μL of chitosan(CS) (1:4) solution were added dropwise on the surface to fix the electrode surface (AChE-CS/PdAu@Co_3O_4-NC/GEC), and placed in a refrigerator at 4℃.

2.5. Ache Sensing Experiment

The AChE-CS/PdAu@Co_3O_4-NC/GEC biosensors were used for OPs detection. Scheme 1 showed the formation process of hollow PdAu@Co_3O_4-NC, as well as it illustrated the efficient approach for pesticides detection. Omethoate and chlorpyrifos were considered as inhibitors of AChE, which could reduce the output of the corresponding hydrolyzed TCl, resulting in a weaker oxidative current. The AChE-CS/PdAu@Co3O4-NC/GEC were soaked in different concentrations of pesticides. The inhibition rates of OPs were estimated as follows: inhibition rate (%) = $(I_0-I_1)/I_0 \times 100\%$, where I_0 and I_1 were the peak currents of ATCl before and after incubation with pesticides.

3. Results And Discussion

3.1. Characterization Of Pdau@coo-nc

The XRD pattern was used to characterize the crystal structure, and the lattice parameters were showed in Fig. S1. The XRD pattern of the synthesized products can be indexed to the spinel Co_3O_4 (JCPDS # 43-1003)[28]. All the sharp and prominent peaks between 5°and 80°match well with that of previous reported X-ray data, clearly indicate that spinel Co_3O_4 is obtained.

The structure and morphology of ZIF-67 and PdAu@Co_3O_4-NC were studied by TEM and SEM. The SEM images in Fig. 1a and the TEM images in Fig. 1c showed that the regular polyhedron shape and side length of the ZIF-67 crystal at approximately was about 500 nm. The TEM in Fig. 1d and the SEM in Fig. 1b showed the size and surface morphology of ZIF-67-derived CoMOF-NH_2. After the reaction, the contours of the rhombic dodecahedron material became blurred (from the Fig. 1b can be seen). The morphology and the size of the CoMOF-NH_2 was similar to the ZIF-67. From the Fig. 1d, these CoMOF-NH_2 exhibited a double-shell structure with no apparent change in shape as compared to ZIF-67. This was because ZIF-67 could react with diaminobisophthalic acid ligand to form CoMOF-NH_2[29]. TEM

images in Fig. 1g and SEM images in Fig. 1e visually illustrate the similar structural profiles of PdAu@CoMOF-NH_2 and CoMOF-NH_2. It can be seen that the PdAuNPs were uniformly distributed on the surface of CoMOF-NH_2, and the high-quality NPs were homogeneous morphology and with the size distribution of about 4 – 8 nm (zhichengcailiao Fig. 1g). After the precursor was heat-treated in air at 300°C (Fig. 1f and Fig. 1h), the polyhedron size changed a little. In the Fig. 1f, the co-based oxides were hollow and the surface becomes rough with holes, showing a unique two-dimensional layered morphology. The TEM image in Fig. 1h further revealed the rough surface of the PdAu@Co_3O_4-NC and the morphology has significantly changed, and the PdAu@CoMOF-NH_2 framework partly collapsed to form PdAu@Co_3O_4-NC. The reasons for the size collapse were the decomposition of organic ligands and the shedding of some functional groups on the surface caused by heat treatment. From the TEM image in Fig. 1h and the Fig. 1i can be seen that the Pd and AuNPs dispersed on the surface of CoMOF-NH_2 with distinct lattice stripes. The interplanar distance was 0.195 nm, which could be attributed to the Pd (200) plane, and the interplanar distance was 0.235 nm, which could be matched to the plane of Au (111). This further confirmed that the bimetallic PdAuNPs were successfully encapsulated on the precursor surface. In addition, the homogeneous distribution of Pd, Au, N, and O elemented in the TEM-mapping images further confirmed the successful synthesis of the target PdAu@Co_3O_4-NC (Fig. 1j).

3.2. Electrochemical Characterization Based On Biosensing Platform

CV and EIS are used to measure different performance characteristics of modified electrodes in 5mM $[Fe(CN)_6]^{3-}$ $/^{4-}$ solution containing 0.1 M KCl. This process was used to investigate the step-by-step fabrication process of PdAu@Co_3O_4-NC electrodes. In Fig. 2a, the PdAu@Co_3O_4-NC and PdAu@CoMOF-NH_2 modified glassy carbon electrodes and exhibited excellent enhancement in peak currents. compared to the glassy carbon electrode. Due to the conductive properties of PdAu@Co_3O_4-NC, the charge transfer rate and the peak current was significantly enhanced. Furthermore, in the AChE/PdAu@Co_3O_4-NC/GCE electrode, a significant drop in the peak current value was observed due to the non-conductive nature of the AChE, and it was also demonstrated that AChE was successfully immobilized on the surface of the electrode. From the EIS analysis (Fig. 2b), it can be seen that the effect of different modification materials on the charge transfer resistance (Rct) in sensor development. It also showed that the electrochemical performance of PdAu@Co_3O_4-NC was excellent. After enzyme immobilization, Rct was increased. Therefore, the electrochemical analysis showed a clear indication of successive modifications, confirming the successfully fabricated biosensor.

3.3. Optimization Of Ache/pdau@coo-nc/gce Platforms

Furthermore, the effect of different conditions on the biosensor was investigated to achieve the best experimental conditions for the DPV response of the biosensor. The pH of the PBS could seriously affect the catalytic activity of immobilized AChE. The pH of the PBS buffer (6.5–8.5) was adjusted to test for

optimal conditions. From Fig. 3a, it can be seen that the current reaches a maximum at the pH of 7.4. Therefore, the optimum pH of the experiment was 7.4 in the subsequent tests.

In addition, the dosage of AChE was also the critical parameter for biosensors. In Fig. 3b, with the increase of AChE dosage, the electrochemical response gradually increased. When the AChE concentration was further increased to 0.2U, the electrochemical response reached the optimum value, and when the AChE concentration exceeded 0.2U, the DPV response decreased relatively. This may be too little AChE will lead to insufficient enzyme catalysis reaction. However, when too much AChE was used to modify the electrode, the modified layer will be too thick, which will hinder the speed of electron transfer and reduce the sensitivity of the biosensor. Thus, in the following experiments, 0.2 U was used as the optimal dosage of AChE. Accordingly, the incubation time also had an important impact on the analytical performance of the enzyme inhibition biosensor. Figure 3c showed the effect of incubation time on the inhibition rate. It can be seen that the inhibition rate gradually increased from 5 min to 25 min, and then remain at a similar level, indicating that the binding of OPs to AChE reaches saturation. Therefore, the optimal inhibition time for pesticides was set to 20 minutes.

3.3. Ache/pdau@coo-nc/gce Platforms Amperometric Response

In order to evaluate the electrochemical response of the constructed AChE biosensor to the ATCl, the time-current curve was tested. Figure 3d was the time-current response curve of AChE-CS/PdAu@Co_3O_4-NC/GCE after continuous addition of the substrate ATCl to the PBS solution. The current response gradually increased with increasing ATCl concentration and stabilized after 2.12 mM. It was worth noticed that the biosensor based on AChE-CS/PdAu@Co_3O_4-NC/GCE exhibited a high response current. This indicated when the composite the electrode surface was modified by PdAu@Co_3O_4-NC, the sensor performance was improved due to the synergistic effect of different components.

Typical amperometric curves of AChE-CS/PdAu@Co_3O_4-NC/GCE sensors were obtained by sequential addition of ATCl to PBS. In Fig. 3e, there was a good linear relationship between the current value (I) and the substrate ATCl concentration (C) in the concentration range of 0.0219 ~ 0.75696mM and 0.89626 ~ 21.12379mM. The corresponding linear regression equations were I(μA) = 0.002 C(μM) + 0.14295(R^2 = 0.99475) and I(μA) = 9.21×10^{-4} C(μM) + 0.94422 (R^2 = 0.98813). Through the Lineweaver-Burk equation [30], the constant of Michaelis-Menten (Km) about AChE-CS/PdAu@Co_3O_4-NC/GCE could be calculated (Fig. 3f). The Km was inversely proportional to the affinity of the AChE to the substrate. In this study, the Km value of the constructed AChE-CS/PdAu@Co_3O_4-NC/GCE biosensors was 67.618 μM, less than 1.56 mM [31], 126 μM [32], 142 μM [33]. As a result, because of the conversion of Co^{3+} to Co^{2+}, the material has good catalytic ability and the porosity of the material can effectively accelerate the electrochemical reaction. This confirmed that the AChE-CS/PdAu@Co_3O_4-NC/GCE had higher affinity and catalytic activity for ATCl.

3.4. Determination Of Omethoate And Chlorpyrifos

The AChE-CS/PdAu@Co_3O_4-NC/GCE electrochemical biosensor was prepared as well as DPV was used to detect trace pesticides under optimized conditions. Drug OPs can covalently bind the activity center of AChE, which reduced peak current from electrochemical oxidation of TCl. Figure 4a and c were the DPV responses of AChE-CS/PdAu@Co_3O_4-NC/GCE incubated with different concentrations of omethoate and chlorpyrifos under optimal assay parameters. With increase concentrations of omethoate and chlorpyrifos, the peak current responses varying from 6.125×10^{-15} to 6.125×10^{-6} mol/L for omethoate, and from 5.1×10^{-13} to 5.1×10^{-6} mol/L for chlorpyrifos. In Fig. 4b, the inhibition rate (I%) is proportional to the logarithm of the omethoate concentration (LogC), and the linear regression equation is I% = 8.23 LogC + 125.90 (R^2 = 0.9984), and the detection limit (LOD) was 6.125×10^{-15} mol/L. The Fig. 4d showed that the linear regression equation of chlorpyrifos is I% = 5.62 LogC + 85.85 (R^2 = 0.995), and the LOD was 5.1×10^{-14} mol/L. Under the same conditions, the AChE-CS/Pd@CoMOF-NH_2/GCE and AChE-CS/PdAu@CoMOF-NH_2/GCE achieved LOD was 6.125×10^{-12} mol/L and 6.125×10^{-13} mol/L for omethoate (Fig. S2), respectively. After comparison, it can be concluded that AChE-CS/PdAu@Co_3O_4-NC/GCE had a good linear range and a low detection limit. This is attributed to the synergistic effect of Pd and Au and the excellent electrical conductivity. Moreover, the hollow structure of Co_3O_4-NC and the stomata on its surface facilitated the transfer of ions and small molecules. Table 1 summarized the performance comparison of AChE-CS/PdAu@Co_3O_4-NC/GCE biosensor with other AChE biosensors, and the results showed that the as-prepared biosensor had comparable or even lower LOD and more wide detection range. There are several possible reasons for the good analytical performance of AChE-CS/PdAu@Co_3O_4-NC/GCE. The porous hollow structural structure provided additional sites for the immobilisation of acetylcholinesterase. In addition, the introduction of PdAuNPs gave the Co_3O_4-based material good electrical conductivity. Above all, the AChE-CS/PdAu@Co_3O_4-NC/GCE had excellent affinity and catalytic activity for ATCl.

The prepared biosensor was applied to the detection of pesticides in real samples to further evidence the practicability. The tap water was used as the sample for testing, and the standard addition method was used for the recovery experiment. After calculation, it can be concluded that the relative standard deviation (RSD) is 1.81% ~ 2.52% and the acceptable recovery is 93.17% ~ 108.25%, indicating that the developed biosensor is feasible and sensitive for monitoring pesticides in real samples (see Table 2).

Table 1
Comparison of the detection performance of AChE-CS/PdAu@Co_3O_4-NC/GCE with other reported biosensors for oxytetracycline and chlorpyrifos.

Sensor	Linear ranges	LOD	Pesticide	Ref
AChE-CS/Au-Tb NSs/GCE	10^{-13}-10^{-7} M	1.26×10^{-14} M	omethoate	[34]
Fe_3O_4@GO and Copper Nanoparticles	5–200 nmol/L	2.48×10^{-9} M	omethoate	[35]
BSA/Apt/rGO-CuNPs/SPCE	1×10^{-11} – 1×10^{-6}M	0.003-0.3 nM	omethoate	[36]
AChE-CS/PdAu@Co_3O_4-NC/GCE	6.125×10^{-15}-6.125×10^{-6}M	6.125×10^{-15}M	omethoate	This work
BSA/AChE/GA/CIS/rGO/SPCE	0.5–470 ng mL^{-1}	0.023 ng mL^{-1}	chlorpyrifos	[24]
AChE/Pin_5COOH/Fe_3O_4NP/GCE	1.5–70 nM	1.5 nM	chlorpyrifos	[37]
MnFe-MOF/SPE	1.0×10^{-9} – 1.0×10^{-7} M	0.85 nM	chlorpyrifos	[38]
AChE-CS/PdAu@Co_3O_4-NC/GCE	5.1×10^{-13} – 5.1×10^{-6}M	5.1×10^{-14}M	chlorpyrifos	This work

3.5. Reproducibility, Anti-interferences And Tability

To investigate the reproducibility and repeatability of the electrochemical sensor, we produced five independent experiments to monitor of omethoate under constant conditions. Based on the electrochemical test result, the RSD of the five independent electrodes were 1.37%, 2.06%, 2.16%, 1.96% and 1.78% (each electrode was used for five replicate DPV experiments), indicating that the biosensor we constructed had good repeatability. The RSD of five different electrodes is 1.26%, which further indicated that the AChE-CS/PdAu@Co_3O_4-NC/GCE has good reproducibility .

Table 2
AChE-CS/PdAu@Co3O4-NC/GCE biosensor to detect the omethoate and chlorpyrifos with tap water.

Pesticide	Add(M)	Detected (M)	Recovery(%)	RSD (%)
omethoate	1.0×10^{-11}	1.0825×10^{-11}	108.25	1.78
omethoate	1.0×10^{-12}	1.0191×10^{-12}	101.90	2.50
omethoate	1.0×10^{-13}	0.9317×10^{-13}	93.17	1.54
chlorpyrifos	5.1×10^{-11}	5.2115×10^{-11}	102.19	2.04
chlorpyrifos	5.1×10^{-12}	4.9851×10^{-12}	93.17	1.31
chlorpyrifos	5.1×10^{-13}	5.0328×10^{-13}	98.68	2.52

This study focused on the use of AChE electrodes for OPs determination so that the complexity of the matrix interference can often result in a non-enzymatic signal. Hence, to evaluate the anti-interference ability of AChE-CS/PdAu@Co_3O_4-NC/GCE for the detection of OPs, experiments were carried out via the addition of some common interfering species such as Zn^{2+} Mg^{2+} Hg^{2+} NO^{3-} PO_4^{3-} Cl^- glucose and citric acid into PBS with 1 mM ATCl. No significant change in current response was observed when an excess of interfering species was added (Fig. 5). Thus, the AChE-CS/PdAu@Co_3O_4-NC/GCE biosensor showed excellent anti-interference for the determination of OPs.

To test the stability of AChE-CS/PdAu@Co_3O_4-NC/GCE sensor, the AChE electrodes were stored in a dry environment at 4°C for 7 days and 30 days, respectively. The AChE-CS/PdAu@Co_3O_4-NC/GCE still maintained 90.84% of the initial current response after 7 days, and even after 30 days reached 82.33%, illustrating the excellent stability of the AChE-CS/PdAu@Co_3O_4-NC/GCE sensor.

4. Conclusion

In summary, we have developed a PdAu@Co_3O_4-NC based AChE biosensor and used it for the highly sensitive determination of pesticides. The electron transfer capability and corresponding electrochemical properties are further improved due to the synergistic effect of Co_3O_4-NC and PdAuNPs. Meanwhile, the hollow and microporous structure of PdAu@Co_3O_4-NC greatly accelerated the current transfer and effectively improved the catalytic performance of AChE. Through optimized conditions, using oxomethoate and chlorpyrifos as model pesticides, the AChE-CS /PdAu@Co_3O_4-NC/GCE biosensor achieved a wide linear detection range and a low detection limit. In addition, the developed biosensor got excellent storage stability, anti-interference and good detection effect in water samples. The results showed that the biosensor had great potential in the detection of OPs as well as the field analysis of other environmental pollutants.

Declarations

Acknowledgments

The authors acknowledge financial support from the National Natural Science Foundation of China (Grant No. 21875205).

Author Contribution

Y.Z., X.L. and F.G. wrote the main manuscript text and Y.Z., J.L., W.G. and C.Z. prepared samples. All authors reviewed the manuscript.

Data Availability statement

Data will be made available on request.

Conflict of Interest

The authors declare no competing financial interests.

References

1. R. Pandiselvam, R. Kaavya, Y. Jayanath, K. Veenuttranon, P. Lueprasitsakul, V. Divya, et al., Ozone as a novel emerging technology for the dissipation of pesticide residues in foods–a review, Trends in Food Science & Technology, 97(2020) 38-54.
2. M. Nehra, N. Dilbaghi, G. Marrazza, A. Kaushik, C. Sonne, K.H. Kim, et al., Emerging nanobiotechnology in agriculture for the management of pesticide residues, J Hazard Mater, 401(2021) 123369.
3. J. Zhang, J. Wang, G.S. Zhou, Y.J. Tan, H.J. Tao, J.Q. Chen, et al., Studies of the Anti-amnesic Effects and Mechanisms of Single and Combined Use of Donepezil and Ginkgo Ketoester Tablet on Scopolamine-Induced Memory Impairment in Mice, Oxid Med Cell Longev, 2019(2019) 8636835.
4. G.E. Fenoy, W.A. Marmisolle, O. Azzaroni, W. Knoll, Acetylcholine biosensor based on the electrochemical functionalization of graphene field-effect transistors, Biosens Bioelectron, 148(2020) 111796.
5. W. Wang, X. Wang, N. Cheng, Y. Luo, Y. Lin, W. Xu, et al., Recent advances in nanomaterials-based electrochemical (bio)sensors for pesticides detection, TrAC, Trends Anal Chem, 132(2020).
6. C.N. Kesavachandran, M. Fareed, M.K. Pathak, V. Bihari, N. Mathur, A.K. Srivastava, Adverse health effects of pesticides in agrarian populations of developing countries, Rev Environ Contam Toxicol, 200(2009) 33-52.
7. R.C. da Silva, V.G. Zuin, J.H. Yariwake, M.N. Eberlin, F. Augusto, Fiber introduction mass spectrometry: determination of pesticides in herbal infusions using a novel sol-gel PDMS/PVA fiber for solid-phase microextraction, J Mass Spectrom, 42(2007) 1358-62.

8. I.P. Rivas, M.E. Gil-Alegre, A.I. Torres-Suárez, Development and validation of a fast high-performance liquid chromatography method for the determination of microencapsulated pyrethroid pesticides, Anal Chim Acta, 557(2006) 245-51.
9. B. Chen, F.-q. Wu, W.-d. Wu, B.-h. Jin, L.-q. Xie, W. Feng, et al., Determination of 27 pesticides in wine by dispersive liquid–liquid microextraction and gas chromatography–mass spectrometry, Microchem J, 126(2016) 415-22.
10. R. Umapathi, S.M. Ghoreishian, S. Sonwal, G.M. Rani, Y.S. Huh, Portable electrochemical sensing methodologies for on-site detection of pesticide residues in fruits and vegetables, Coord Chem Rev, 453(2022).
11. S. Yang, J. Liu, H. Zheng, J. Zhong, J. Zhou, Simulated revelation of the adsorption behaviours of acetylcholinesterase on charged self-assembled monolayers, Nanoscale, 12(2020) 3701-14.
12. J. Cao, M. Wang, H. Yu, X. Jing, Y. X. She, C. Zhen, et al., An overview on the mechanisms and applications of enzyme inhibition-based methods for determination of organophosphate and carbamate pesticides, JOURNAL OF AGRICULTURAL AND FOOD CHEMISTRY, 68(2021)7298-7315.
13. R. Liu, L. Jiang, Z. Yu, X. Jing, X. Liang, D. Wang, et al., MXene (Ti_3C_2T)-Ag nanocomplex as efficient and quantitative SERS biosensor platform by in-situ PDDA electrostatic self-assembly synthesis strategy, Sensors and Actuators B: Chemical, 333(2021).
14. Y. Xie, X. Tu, X. Ma, Q. Fang, G. Liu, R. Dai, et al., A CuO-CeO_2 composite prepared by calcination of a bimetallic metal-organic framework for use in an enzyme-free electrochemical inhibition assay for malathion, Mikrochim Acta, 186(2019) 567.
15. B. Wang, Y. Li, H. Hu, W. Shu, L. Yang, J. Zhang, Acetylcholinesterase electrochemical biosensors with graphene-transition metal carbides nanocomposites modified for detection of organophosphate pesticides, PLoS One, 15(2020) e0231981.
16. P. Liu, X. Li, X. C. Xu, K. Ye, L. J. Wang, H. J. Zhu, et al., Integrating peroxidase-mimicking activity with photoluminescence into one framework structure for high-performance ratiometric fluorescent pesticide sensing, Sensors and Actuators B: Chemical, 328 (2021).
17. J. Fu, Sensitive Acetylcholinesterase Biosensor Based on Screen- Printed Carbon Electrode Modified with Cerium Oxide- Chitosan/Mesoporous Carbon-Chitosan for Organophosphorus Pesticide Residue Detection, International Journal of Electrochemical Science, (2018) 9231-41.
18. E. Mahmoudi, H. Fakhri, A. Hajian, A. Afkhami, H. Bagheri, High-performance electrochemical enzyme sensor for organophosphate pesticide detection using modified metal-organic framework sensing platforms, Bioelectrochemistry, 130(2019) 107348.
19. C. Li, S. Li, J. Zhao, M. Sun, W. Wang, M. Lu, et al., Ultrasmall Magneto-chiral Cobalt Hydroxide Nanoparticles Enable Dynamic Detection of Reactive Oxygen Species in Vivo, J Am Chem Soc, 144(2022) 1580-8.
20. R. Chen, Y. Tan, Z. Zhang, Z. Lei, W. Wu, N. Cheng, et al., Hydrazine Hydrate Induced Two-Dimensional Porous Co^{3+} Enriched Co_3O_4 Nanosheets for Enhanced Water Oxidation Catalysis, ACS Sustainable Chemistry & Engineering, 8(2020) 9813-21.

21. Y. Zheng, Z. Liu, H. Zhan, J. Li, C. Zhang, Studies on electrochemical organophosphate pesticide (OP) biosensor design based on ionic liquid functionalized graphene and a Co_3O_4 nanoparticle modified electrode, Analytical Methods, 8(2016) 5288-95.
22. A.L. Wang, H. Xu, J.X. Feng, L.X. Ding, Y.X. Tong, G.R. Li, Design of Pd/PANI/Pd sandwich-structured nanotube array catalysts with special shape effects and synergistic effects for ethanol electrooxidation, J Am Chem Soc, 135(2013) 10703-9.
23. Y. Wang, X. L, Geoffrey I.N. Waterhouse, Y. L. Zhou, H. S. Yin, et al., Photoelectrochemical biosensor for protein kinase A detection based on carbon microspheres, peptide functionalized Au-ZIF-8 and TiO_2/g-C_3N_4, Talanta: Chemical, 196(2019) 197-203.
24. F. Liu, J. Peng, Y.-M. Lei, R.-S. Liu, L. Jin, H. Liang, et al., Electrochemical detection of ctDNA mutation in non-small cell lung cancer based on CRISPR/Cas12a system, Sensors and Actuators B: Chemical, 362(2022).
25. X. Lu, L. Tao, D. D. Song, Y. Li, F. M. Gao, Bimetallic Pd@Au nanorods based ultrasensitive acetylcholinesterase biosensor for determination of organophosphate pesticides, Sensors and Actuators B: Chemical, 255 (2018) 2575–2581.
26. T. Itsoponpan, C. Thanachayanont, P. Hasin, Sponge-like $CuInS_2$ microspheres on reduced graphene oxide as an electrocatalyst to construct an immobilized acetylcholinesterase electrochemical biosensor for chlorpyrifos detection in vegetables, Sensors and Actuators B: Chemical, 337(2021).
27. Y. Zhao, X. Li, J. Chen, X. Lu, Y. Yang, D. Song, et al., Porous hierarchical peony-like cobalt-based bimetallic oxides structured by ultrathin nanosheets for highly sensitive electrochemical pesticides detection, Sensors and Actuators B: Chemical, 352(2022).
28. S. Tangestaninejad, P. Horcajada, M. Moghadam, V. Mirkhani, I.Mohammadpoor-Baltork, R. Kardanpour, F. Zadehahmadi, Efficient biodiesel production using a lipase@ZIF-67 nanobioreactor, Chemical Engineering Journal, (2017)
29. X. Deng, L. Yang, H. Huang, Y. Yang, S. Feng, M. Zeng, et al., Shape-Defined Hollow Structural Co-MOF-74 and Metal Nanoparticles@Co-MOF-74 Composite through a Transformation Strategy for Enhanced Photocatalysis Performance, Small, 15(2019) e1902287.
30. W. Yang, X. Zhou, N. Zheng, X. Li, Z. Yuan, Electrochemical biosensors utilizing the electron transfer of hemoglobin immobilized on cobalt-substituted ferrite nanoparticles–chitosan film, Electrochim Acta, 56(2011) 6588-92.
31. B. Zou, Y. Chu, J. Xia, Monocrotophos detection with a bienzyme biosensor based on ionic-liquid-modified carbon nanotubes, Anal Bioanal Chem, 411(2019) 2905-14.
32. Y.S. Zhao, X. Zuo, X. Lu, Z.P. Li, F.M. Gao, Hierarchical porous hollow N-doped Cu-based MOF derivatives as highly sensitive electrochemical sensing platform for pesticides detection, Sensors and Actuators B-Chemical, 362(2022).
33. D. Song, X. Jiang, Y. Li, X. Lu, S. Luan, Y. Wang, et al., Metal-organic frameworks-derived MnO2/Mn3O4 microcuboids with hierarchically ordered nanosheets and Ti_3C_2 MXene/Au NPs composites for electrochemical pesticide detection, J Hazard Mater, 373(2019) 367-76.

34. Y. Yang, Y. Zhao, F. Sun, T. You, Y. Gao, P. Yin, Electrochemically synthesized superhydrophilic 3D tree-like Ag microstructure for ultrasensitive detection of omethoate, Microchem J, 159(2020).
35. H. Zhang, W.-K. Kang, Y. Wang, X.-Z. Wang, L.-H. Lu, An Enzymatic Reaction Modulated Fluorescence-on Omethoate Biosensor Based on Fe_3O_4@GO and Copper Nanoparticles, Journal of Analysis and Testing, 6(2022) 3-11.
36. J. Y. Fu, X. Li, X. S. An, Y. Yao, Y. Yang, Y. Guo, et al., Electrochemical aptasensor based on one step co-electrodeposition of aptamer and GO-CuNPs nanocomposite for organophosphorus pesticide detection, Sensors and Actuators B: Chemical, 287(2019).
37. N. Chauhan, J. Narang, U. Jain, Amperometric acetylcholinesterase biosensor for pesticides monitoring utilising iron oxide nanoparticles and poly(indole-5-carboxylic acid), Journal of Experimental Nanoscience, 11(2015) 111-22.
38. P. Janjani, U. Bhardwaj, R. Gupta, H. Singh Kushwaha, Bimetallic Mn/Fe MOF modified screen-printed electrodes for non-enzymatic electrochemical sensing of organophosphate, Anal Chim Acta, 1202(2022) 339676.

Scheme

Scheme 1 is available in the Supplementary Files section.

Figures

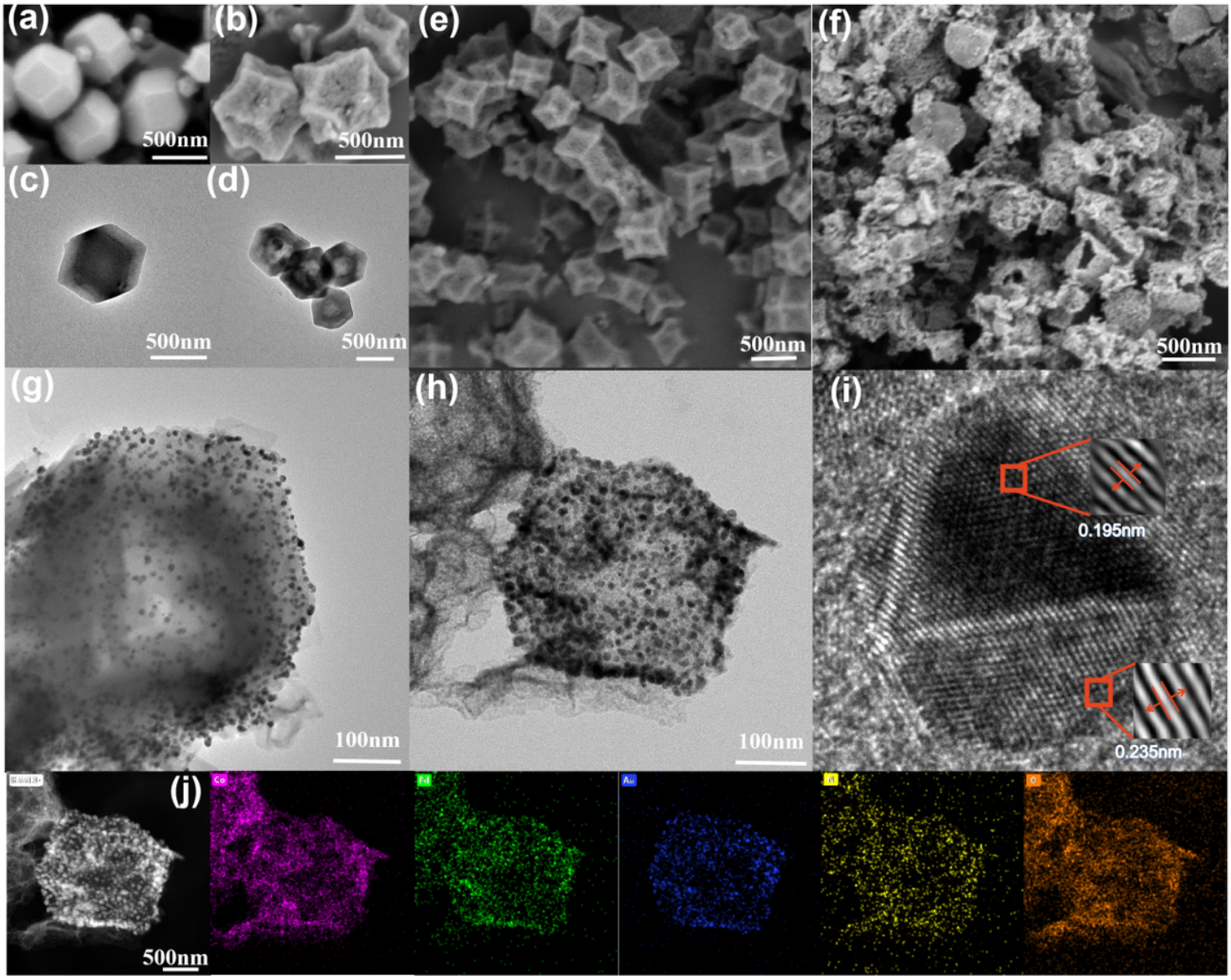

Figure 1

SEM images of (a)ZIF-67, (b) CoMOF-NH_2, (e) PdAu@CoMOF-NH_2 and (f) PdAu@Co_3O_4-NC. TEM images of (c)ZIF-67, (d) CoMOF-NH_2, (g) PdAu@CoMOF-NH2 and (h) PdAu@Co_3O_4-NC and (i) HRTEM images of PdAu@Co_3O_4-NC. (j) TEM elemental mapping images of PdAu@Co_3O_4-NC.

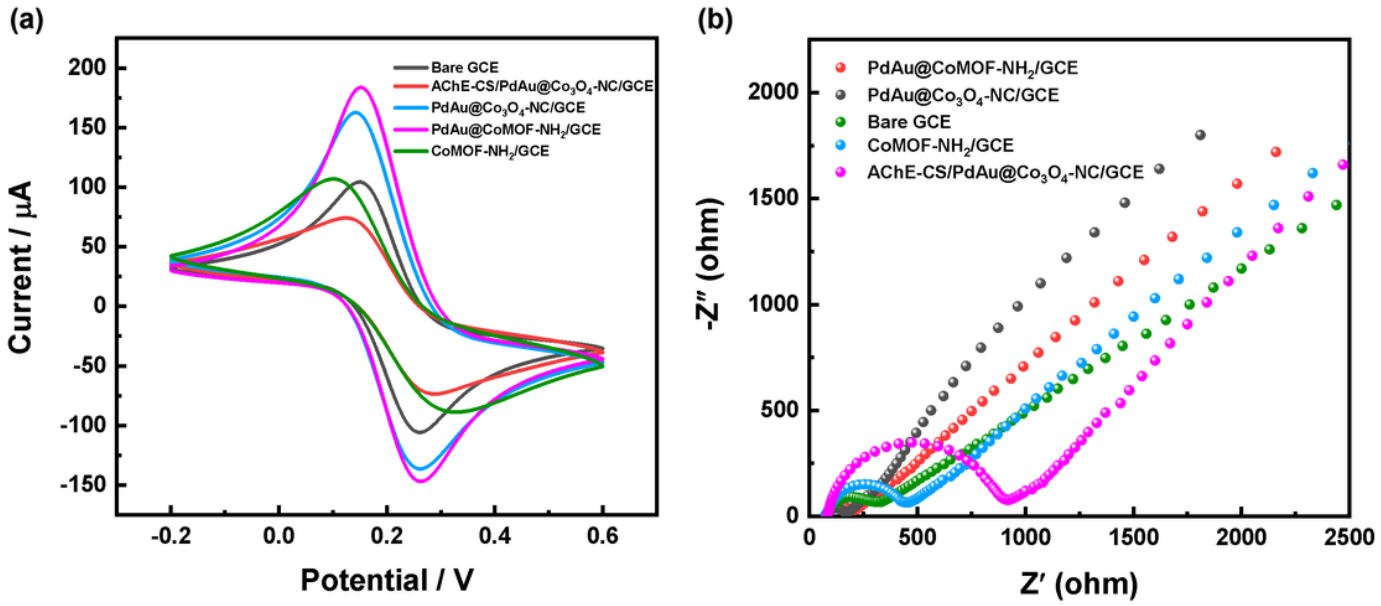

Figure 2

(a) CV characterization of the electrodes in in 5mM $[Fe(CN)_6]^{3-/4-}$ solution containing 0.1 M KCl. (b) EIS Nyquist plots of the electrodes in 5mM $[Fe(CN)_6]^{3-/4-}$ solution containing 0.1 M KCl.

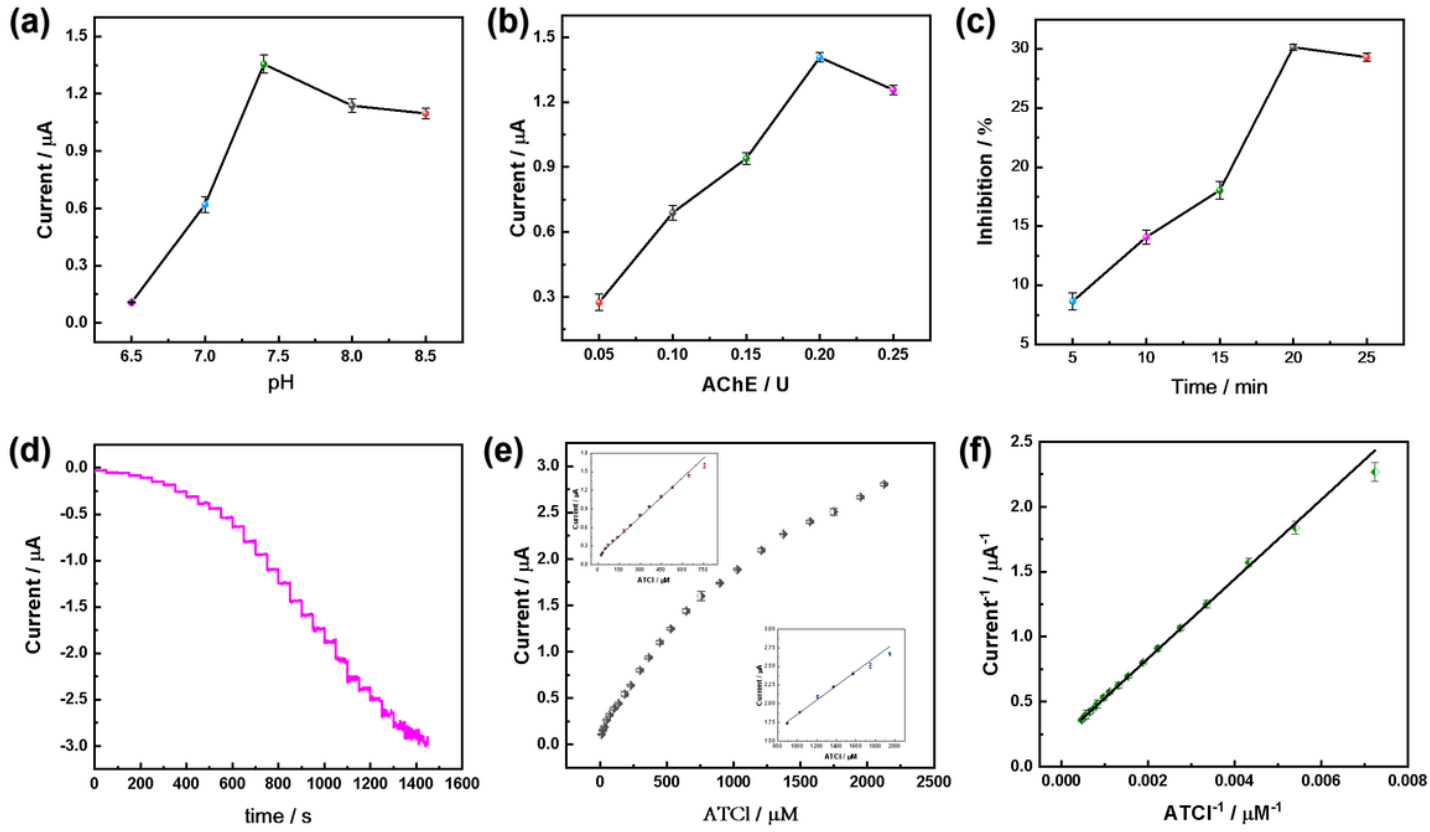

Figure 3

(a)Effects of pH, (b)Effect of AChE amounts, and (c)incubation time on the performance of the developed biosensor. (d) Amperometric responses of by successive addition of ATCl in 0.1 M and pH 7.4 PBS with a mild stirring. (e) Calibration curve for ATCh determination. (f) The Lineweaver-Burk plot of 1/I. 1/C.

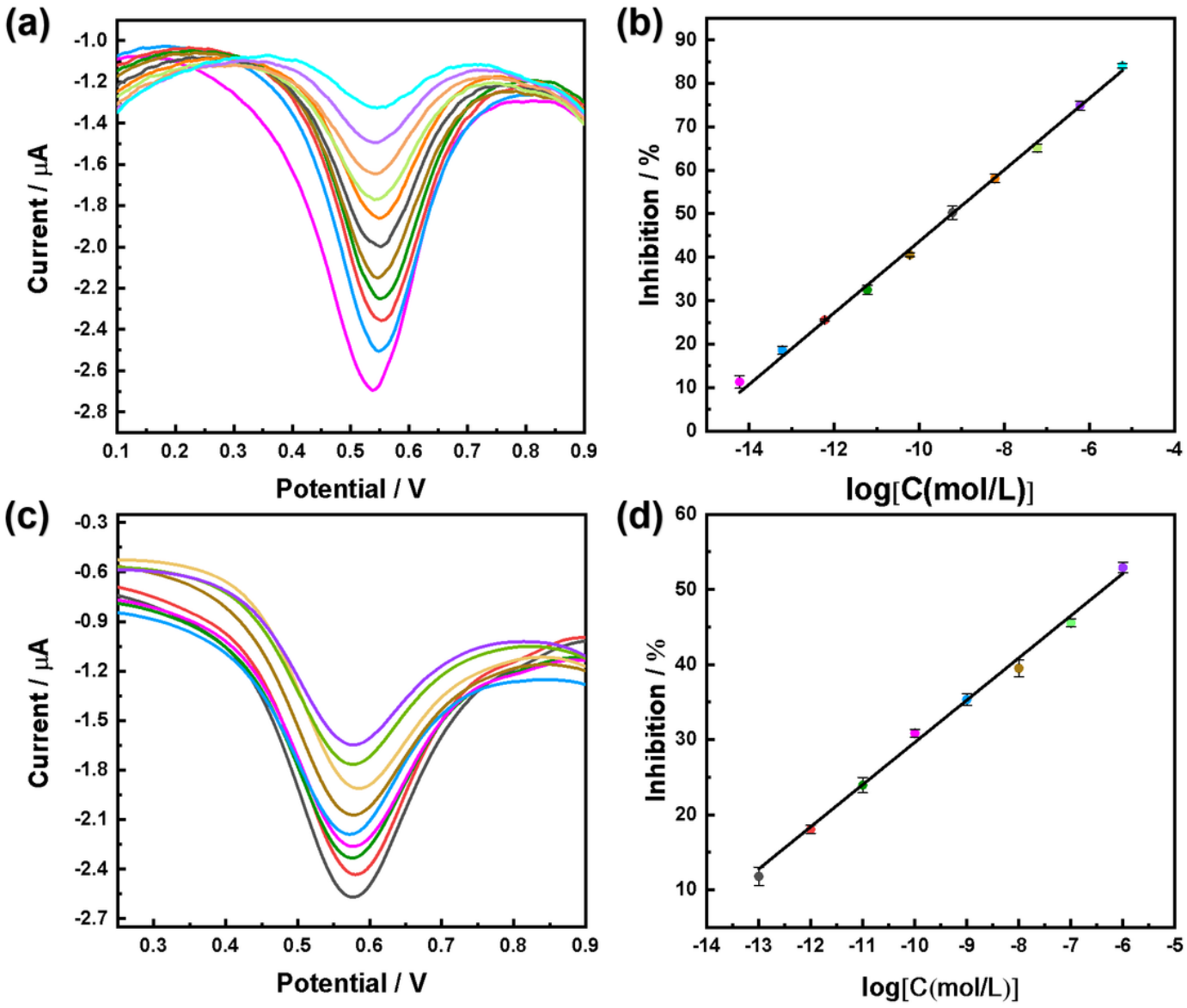

Figure 4

Different concentrations of omethoate (a) and chlorpyrifos (b) inhibit the DPV response of AChE-CS/PdAu@Co_3O_4-NC/GCE biosensor; Calibration chart of omethoate (b) and chlorpyrifos (d).

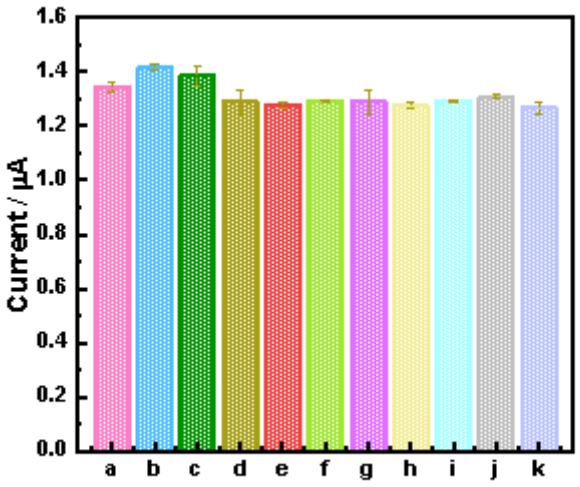

Figure 5

AChE/ PdAu@Co_3O_4-NC/GCE towards 1.0 mM ATCl in the presence/absence of interfering substances(a-ATCl，b-glucose，c-citric acid，d-Zn^{2+}，e-Mg^{2+}，f-Fe^{3+}，g-SO_4^{2-}，h-NO_3^-，i-PO_4^{3-}，j-Cl^-，k-carbamide).

Supplementary Files

This is a list of supplementary files associated with this preprint. Click to download.

- SupportingInformation1.docx
- Scheme1.png